Flexible Platform for *In Situ* Impedimetric Detection and Bioelectric Effect Treatment of *Escherichia Coli* Biofilms

Ryan C. Huiszoon [ORCID], Sowmya Subramanian, Pradeep Ramiah Rajasekaran, Luke A. Beardslee,
William E. Bentley, and Reza Ghodssi [ORCID], *Fellow, IEEE*

Abstract—*Goal:* **This paper reports a platform for real-time monitoring and treatment of biofilm formation on three-dimensional biomedical device surfaces.** *Methods:* **We utilize a flexible platform consisting of gold interdigitated electrodes patterned on a polyimide substrate. The device was integrated onto the interior of a urinary catheter and characterization was performed in a custom-developed flow system. Biofilm growth was monitored via impedance change at 100 Hz ac with a 50 mV signal amplitude.** *Results:* **A 30% impedance decrease over 24 h corresponded to *Escherichia coli* biofilm formation. The platform also enabled removal of the biofilm through the bioelectric effect; a low concentration of antibiotic combined with the applied ac voltage signal led to a synergistic reduction in biofilm resulting in a 12% increase in impedance. Biomass characterization via crystal violet staining confirmed that the impedance detection results correlate with changes in the amount of biofilm biomass on the sensor. We also demonstrated integration with a chip-based impedance converter to enable miniaturization and allow *in situ* wireless implementation. A 5% impedance decrease measured with the impedance converter corresponded to biofilm growth, replicating the trend measured with the potentiostat.** *Conclusion:* **This platform represents a promising solution for biofilm infection management in diverse vulnerable environments.** *Significance:* **Biofilms are the dominant mode of growth for microorganisms, where bacterial cells colonize hydrated surfaces and lead to recurring infections. Due to the inaccessible nature of the environments where biofilms grow and their increased tolerance of antimicrobials, identification, and removal on medical devices poses a challenge.**

Index Terms—**Bacterial biofilm, bioelectric effect, flexible device, impedance sensor, medical implants.**

I. INTRODUCTION

BACTERIAL biofilms are ubiquitous in healthcare and the environment, representing the dominant mode of growth for bacterial microorganisms [1]. Biofilms present a significant challenge because they afford bacteria significant survival advantages compared to their planktonic counterparts, including increased tolerance to antimicrobial therapies [2], [3]. Biofilms are implicated in numerous nosocomial infections, including surgical-site, bloodstream, and urinary tract infections associated with medical implants, venous catheters, or urinary catheters, respectively [4]. Overall, these are estimated to be responsible for 62% of all hospital-acquired infections [5]. Furthermore, bacterial biofilms are the primary cause of nosocomial urinary tract infections, infecting catheterized patients at a rate of 5–7% per day of implantation [6]. Due to limited diffusion into the biofilm matrix and the decreased metabolic rate of the constituent bacteria, biofilm bacteria become highly tolerant to antibiotic therapy; an antibiotic dose 500–5000 times larger than that for planktonic bacteria is required to eliminate the biofilm and associated infection [2], [3].

Bacteria form sessile biofilm communities when they adhere to a hydrated surface such as that of a urinary catheter, and, at a threshold population, encase themselves in a self-produced extracellular matrix (ECM) consisting primarily of polysaccharides and extracellular DNA [1], [2]. The adhered bacteria communicate via small molecules through a process called quorum sensing, where they coordinate their mode of growth [7]. The biofilm will continue to develop into a complex structure from which bacteria disperse throughout the environment. These dispersed bacteria allow additional areas of the system to be colonized by biofilm, and can serve as a source of persistent infections if the original biofilm is not removed [2]. This leaves catheters or medical implants susceptible to recurring infections that can only be treated by removing the implant, often requiring revisional surgery [8]. Early detection of biofilm formation, along with novel prevention and treatment schemes, will thus allow for prevention of these recurring infections.

Conventional techniques for biofilm analysis include colony counting on agar plates [9] or staining with dyes or fluorescent markers [10]. Colony counting relies on gathering samples and requires hours or days for growth before results are determined. In addition, this only quantifies the presence of bacterial cells and not the formation of a biofilm [9]. Staining requires optical equipment such as fluorescence microscopes or spectrophotometers for analysis, and thus does not lend itself to interfacing with various systems vulnerable to biofilms. Confocal

microscopy, in particular, has emerged as an integral technique for biofilm research that enables detailed 3D imaging. However, this technique requires expensive and bulky equipment, limiting its utility directly in affected environments [11]. The slow and indirect nature of these methods for evaluating biofilm have motivated researchers to develop new techniques for real-time and *in situ* analysis.

Numerous sensing schemes have been proposed in recent years for more effective biofilm monitoring. These include surface acoustic wave sensors [12], tuning fork resonators [13], and optical density monitoring platforms [14], [15]. These methods are not easily translated to *in vivo* settings due to the complexity of the geometry and dynamic environment where biofilm sensing is desirable, such as on the cylindrical lumen of a catheter or the surface of an artificial knee prosthesis. Electrochemical techniques utilizing microelectrodes have also generated significant interest for their potential as tools for monitoring biofilm formation, particularly impedimetric sensors. The system impedance of a two-electrode biofilm sensor has been shown to effectively monitor biofilm formation non-destructively and in real-time as biofilm forms directly on the electrode surface [16]–[20]. Biofilm alters the capacitive and resistive characteristics of the sensor, leading to measurable change in overall impedance. Interdigitated electrode (IDE) patterns are a common arrangement for impedance sensor microelectrodes, offering the advantage of sensitivity and compact size, as well as tunability based on the width and spacing of the IDE fingers [16]. In addition, different information about the biofilm can be acquired depending on the measurement signal frequency interrogated [21]. However, existing IDE impedance sensors do not lend themselves to *in situ* analysis directly on vulnerable surfaces.

In addition to detection of bacterial biofilm, it is equally important to integrate an approach that addresses prevention or removal. Conventional biofilm infection management relies on systemic antibiotics, which may exacerbate the spread of antibiotic resistant strains, and are often ineffective against biofilm colonies due to their increased tolerance of antibiotics. Several approaches have been developed to address persistent infections caused by biofilm formation, including anti-biofilm surface modifications and coatings [22]–[27], quorum sensing inhibitors [28]–[30], and electric-field based approaches [31]–[35]. In particular, the bioelectric effect (BE), an electric field-based method, was first described over twenty years ago as the combination of a low intensity electric field and antimicrobial to achieve a synergistic killing of biofilm bacteria [32], [36]. This principle enables near-minimum inhibitory concentration (MIC) levels of antibiotic to be effective in biofilm treatment, when they would otherwise have no discernible effect. Although an exact general mechanism has not been established, a variety of hypotheses have been suggested to describe the phenomenon, including electrophoretic augmentation of antimicrobial penetration into the biofilm [32], disruption of the biofilm matrix binding to antimicrobial compounds [36], generation of oxygen [37], potentiating oxidants or reactive oxygen species [38], or generation of reactive chlorine [39]. Previous works from our group have demonstrated BE in microfluidic systems utilizing integrated microelectrodes [16], [40]. Importantly, numerous electric field-based biofilm treatment strategies have emerged from the above works which show promise for utilization in a complete biofilm management system.

In this work, we report a flexible impedance sensor capable of detecting biofilm formation in a cylindrical setting, specifically in the interior lumen of a catheter. The device is comprised of gold IDEs fabricated on polyimide film, allowing the electrodes to conform to the 3D curved surfaces of medical devices to sense biofilm in real-time. The highly flexible nature of the thin polyimide film encourages facile integration with the cylindrical architecture of the catheter lumen, and it is both biologically inert and compatible with microelectronic fabrication processes [41]. The platform was characterized in a custom flow system consisting of a catheter tube integrated with the device on which biofilm was grown. We characterized the impedance sensor response measured using a benchtop potentiostat, as well as a chip-based impedance converter. Impedance sensing with the impedance converter enables miniaturization, an important step for practical implementation of *in situ* wireless biofilm management. In addition to biofilm detection during growth, we demonstrate removal of biofilm using BE, which reduces the concentration of antibiotics required for biofilm elimination. The same electric field introduced for impedance sensing was utilized to implement BE treatment. This allows the flexible platform to serve as a vehicle for continuous monitoring of the catheter surface with regard to biofilm colonization while significantly reducing the medical burden of the infection without excessive antibiotic use.

II. METHODS

A. Flexible Impedance Sensor Fabrication

The electrodes were patterned on the polyimide substrate using a standard photolithography process. A 25.4 μm thick Kapton HD polyimide film (McMaster-Carr) was affixed to the surface of a 4-inch silicon wafer via heat-release tape (Semiconductor Equipment Corp.). A photolithography step with a positive resist (Shipley 1813 resist, Microchem) defined the electrode geometry on the polyimide substrate. Each patterned polyimide substrate was then exposed to oxygen plasma for 1 minute at 200 W immediately prior to metal deposition to improve adhesion. 20/200 nm of chromium/gold was deposited on the wafer via e-beam evaporation (Angstrom Engineering), with the chromium serving as an adhesion layer. Electrode fabrication was completed via a lift-off step in acetone for 1 minute. The electrode patterned polyimide substrate was removed from the wafer by heating to 150 °C on a hot plate, prompting release by the tape. The fabrication process is depicted in Fig. 1.

Each device consisted of gold IDEs with width and spacing of 300 μm over a 10 mm × 40 mm footprint, connected to 30 mm-long gold leads. The device schematic is shown in Fig. 2(a), along with a photograph of the actual device integrated with catheter tubing in Fig. 2(b).

B. Flow System Preparation and Conditioning

The new custom-designed flow system is depicted in Fig. 3 and consists of two 500 ml flasks, with one serving as a media reservoir and the other as a waste container. The flasks were
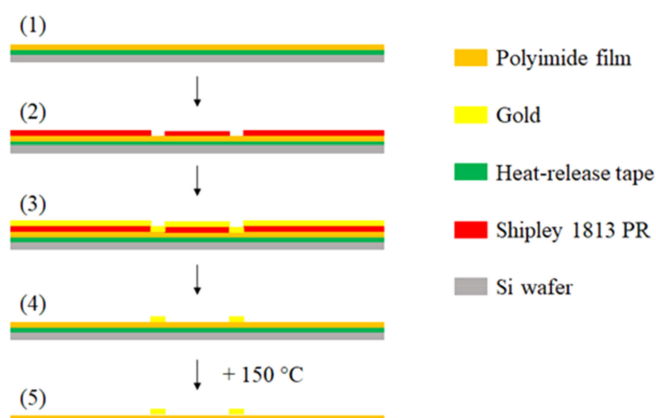
Fig. 1. Fabrication process flow: (1) adhere film to wafer, (2) pattern electrodes, (3) metal deposition, (4) lift-off, and (5) release from tape at 150 °C.

Fig. 2. (a) A schematic of the flexible platform showing 1) the flexible 25.4 μm polyimide substrate, 2) Gold leads for interfacing the sensor with a potentiostat, and 3) Gold IDEs with 300 μm width and spacing over a 10 $\times$ 40 mm² footprint. (b) An optical image of the device interfaced with the interior lumen of the catheter tube (inner diameter of 4.5 mm). The device is seamlessly integrated onto the curved surface with no signs of degradation, highlighting the advantage of the flexible platform.
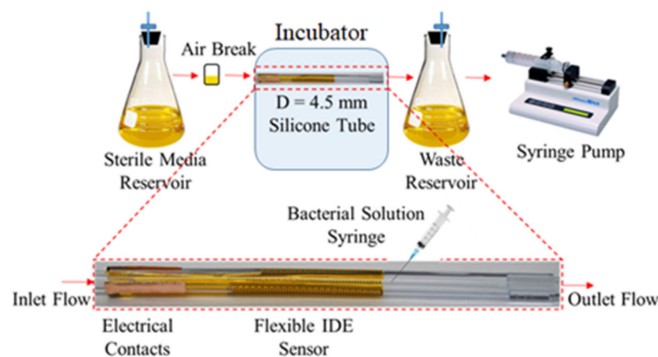

Fig. 3. Custom flow system setup for testing *in situ* biofilm detection and BE treatment in a catheter model.

connected to an 11 cm section of catheter tubing (Allegro Medical) with the sensor adhered. The flasks were sealed with rubber stoppers, with two holes to make fluidic connections. Uncured polydimethylsiloxane (PDMS) (Dow-Corning) mixed at a ratio of 10:1 base to curing agent was coated on the interior of the catheter tube by introducing a large drop at the inlet, and spreading it over the entire surface with a wooden applicator rod. The flexible device was introduced while the surface was coated in uncured PDMS. Throughout the process of adhering the device to the catheter tube surface, the tube was held in a vertical

position to ensure any excess PDMS would flow away from the IDEs. Then, the PDMS was cured for 3 hours at 60 °C to fix the polyimide substrate in place. Once cured, fluidic connections were assembled with tygon tubing and luer connectors (Cole-Parmer), interfacing the sensor and catheter section with the media and waste reservoirs. The media container was filled with 500 ml of Luria broth (LB) media (Sigma). The catheter/sensor system, tubing, and both reservoirs were autoclaved for 40 min at 121 °C for sterilization. The components were then connected in a sterile biosafety cabinet to prevent contamination. The electrical connections were made by sandwiching Al foil in between the contact pads and the tygon tubing. The outer diameter of the tubing and the inner diameter of the catheter tube are such that the connection is friction sealed. This friction seal also served to hold the foil contact in place and isolate it from the solution being flowed. The foil extended beyond the catheter tube on the outside of the tygon tubing, where it could interface with the potentiostat. Following assembly, pure LB media was introduced throughout the flow system for conditioning to remove air pockets. An air break was included to prevent bacteria traveling from the catheter into the sterile media reservoir. The reservoirs were connected to 0.2 μm syringe filters to equalize the pressure during flow and maintain sterility. Flow was driven by a syringe pump in withdrawal mode at 7 ml/h. The sensor/catheter system was maintained at 37 °C in a closed incubator, to simulate an inserted catheter.

C. Biofilm Growth and Treatment

Prior to each experiment, *Escherichia coli* K-12 W3110, a wild-type strain exhibiting a biofilm-forming phenotype, were incubated in 5 ml of LB media for 20 hours at 37 °C in an Innova 4000 incubator shaker (New Brunswick Scientific) set to 250 rpm. The bacterial solution was then diluted to an OD600 of 0.25 (corresponding to 6×10^7 CFU/ml). 1 ml of the diluted bacterial suspension was injected directly into the flow system connected to the catheter-sensor flow system. Bacteria attached to the silicone catheter and sensor surface for 2 hours under static (no flow) conditions, constituting the 'seeding' phase. Following seeding, fresh LB media was flowed through the system at 7 ml/h for 24 hours, constituting the 'growth' phase. Time-lapse images of biofilm growth were acquired using a digital camera (Sony Alpha 6000) at 0, 6, 12, and 24 hour time intervals. Following 24 hours of growth, pure LB media or LB media with 10 μg/ml gentamicin (Fisher Scientific) - a broad spectrum antibiotic - was flowed through at 7 ml/h for an additional 20 hours, constituting the 'treatment' phase. Throughout the experiment, impedance data were collected via a potentiostat (model 660D, CHInstruments) running through a previously-developed MATLAB-based graphical user interface [16]. The impedance spectra from 10 Hz to 10^6 Hz at 50 mV was determined at four different phases of the growth experiments: conditioning with media before the addition of bacteria, seeding, 5 hours into growth, and 24 hours into growth. This allowed characterization of the impedance response due to biofilm growth. The relative percent change in impedance was calculated and compared between an unseeded control and a sample
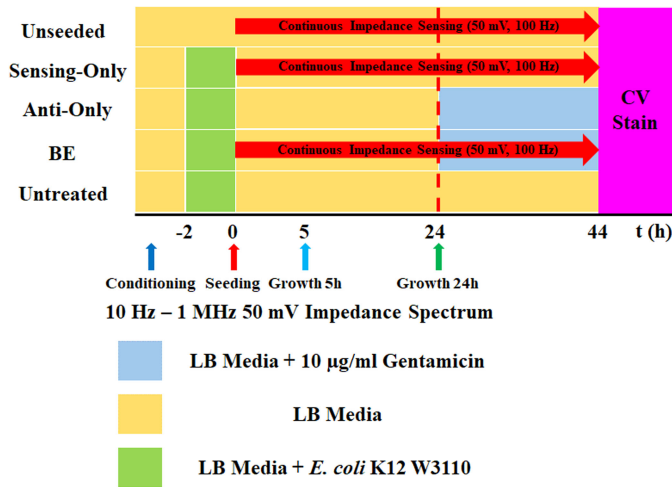
Fig. 4. Experimental conditions and timing showing when treatments were applied and when data was collected.

having biofilm using (1), where Z is the system impedance at the time of measurement and $Z_{initial}$ is the impedance at t = 0. One-way analysis of variance (One-way ANOVA) was performed to evaluate the significance of the changes in impedance.

$$\% \ change \ in \ Z = (Z - Z_{initial}) / Z_{initial} \times 100 \quad (1)$$

In order to evaluate this platform as a real-time monitoring tool, the impedance was measured every 2.25 minutes throughout the growth and treatment phases. Real-time impedance monitoring was also performed with an AD5933 impedance converter (Analog Devices). The 200 mV impedance at 1 kHz was measured every 2 minutes by connecting the device leads to the AD5933 on the UG-364 evaluation board (Analog Devices), utilizing the accompanying evaluation board software. The different sensing parameters were selected due to the limitations of the evaluation board. The 200 mV was the minimum excitation signal possible with board, and the measurements showed the best reproducibility at 1 kHz.

In addition to detection, the platform can be used to implement biofilm treatment based on BE. Five samples were compared to evaluate sensing and BE efficacy: 1) Unseeded, 2) Sensing-only, 3) BE treatment, 4) Antibiotic-only, and 5) Untreated. The unseeded sample served as a negative control, without any bacteria introduced initially. The Sensing-only sample was exposed to the 50 mV sensing signal over the duration of the experiment. BE treatment consisted of the sensing signal, with the gentamicin added for the treatment phase. The Antibiotic-only samples did not have the impedance sensing voltage, but did have gentamicin present during the 20 hours treatment period. An untreated control was seeded with bacteria, but has neither the voltage associated with sensing nor the antibiotic. Only biomass quantification using crystal violet (CV) staining was performed for untreated samples; no impedance sensing was performed on these samples. The relative change in impedance was recorded as a percentage change relative to the initial impedance using (1). The experimental conditions and timing are summarized in Fig. 4.

D. Biofilm Biomass Quantification

The biofilm biomass following the completion of the growth and treatment phases was quantified using a CV absorbance assay. CV stain binds to the extracellular proteins and DNA associated with biofilm formation. CV solution was prepared by adding 50 μg of CV powder (Fisher Scientific) to 10 ml of deionized water. To perform the CV assay, the silicone tube with the sensor was disconnected from the flow system, and one end was sealed with a 3-way stopcock. The tube was drained to remove media and non-adherent cells. The stopcock was sealed and the tube was positioned vertically with the open end directed upward. The tube was then filled via pipette with 1 ml of the 0.0005% weight percentage CV solution and allowed to incubate for 15 minutes. The CV solution was then drained from the tube, and both the tube and sensor were gently rinsed 4 times with 1x PBS to remove unbound CV stain. Following this, the tube was filled with 1 ml of decomplexation solution (4:1 ethanol to acetone) for 30 minutes. CV is soluble in the decomplexation solution, so the CV bound to the biofilm accumulated in the solution and changed its optical density (OD). Finally, the solution in the tube was drained into a cuvette and the biomass was quantified via OD measurements at 590 nm using a UV-visible spectrum spectrophotometer (SpectraMAX). One-way ANOVA was performed to evaluate the significance of the biomass quantification results.

III. RESULTS AND DISCUSSION

A. Biofilm Formation Impedance Sensing

Impedance spectra were obtained and compared at four sequential phases during the biofilm growth process. The average impedance spectra are shown in Fig. 5(a)–(b), and the percent change at each phase relative to the initial impedance measured during the conditioning phase is shown in Fig. 5(c)–(d) for 10 Hz, 100 Hz, 1 kHz, 10 kHz, and 100 kHz. The control sample in Fig. 5(a) was characterized by a relatively uniform increase in impedance across all frequencies, with a small shift apparent after 5 hours and a more significant shift after 24 hours. By contrast, samples with biofilm in Fig. 5(b) were characterized by decreases in impedance at lower frequencies, particularly below 5 kHz. The change was negligible after 5 hours of growth. However, after 24 hours of growth a mature biofilm had formed and the impedance spectrum had shifted at lower frequencies. The control showed an increase in impedance of 20–30% at each of the representative frequencies at the end of the 24 hour period (Fig. 5(c)). This increase was irrespective of frequency and was attributed to the formation of small bubbles near the sensor surface due to the permeability of the silicone to air, which allowed air to diffuse through the tube walls. The formation of small bubbles was further encouraged by the negative pressure created in the tube used to drive the LB media flow. This encouraged bubbles to expand with air from outside the tube. After 24 h of biofilm growth, there was a decrease in impedance of 5–20% at 1 kHz and below (Fig. 5(d)). Overall, the spectra showed significant difference in relative change in impedance with 24 hours of biofilm formation (Fig. 5(d))
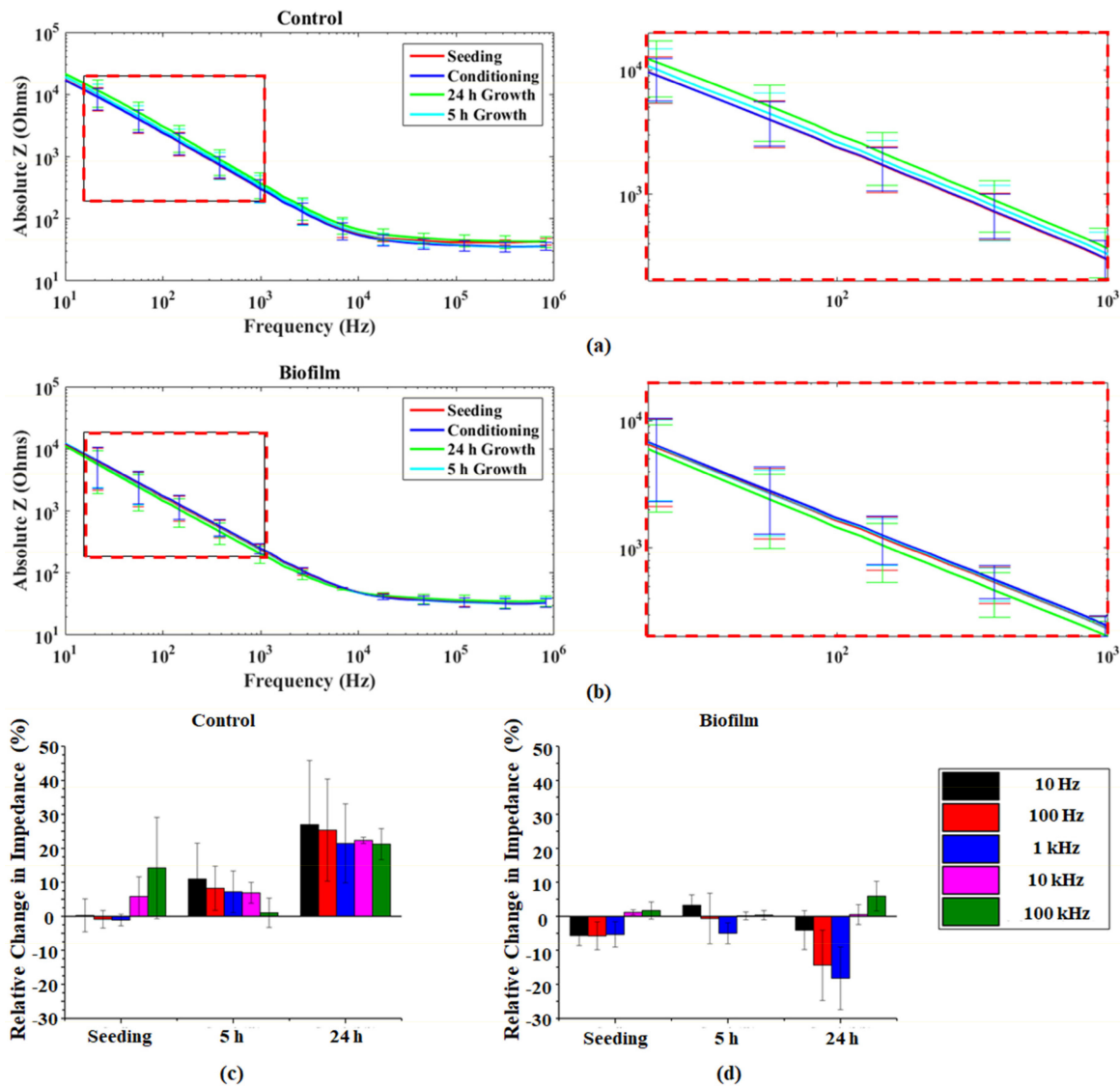
Fig. 5. 50-mV impedance spectra at different intervals throughout biofilm growth experiments, (a) without biofilm (control) and (b) with biofilm formation. The dotted boxes (expanded on the right) highlight the region from 20 Hz to 1 kHz to emphasize the differing responses. Relative percent change in impedance at 5 representative frequencies (c) without biofilm (control) and (d) with biofilm formation. Control samples showed a uniform increase in impedance compared to a distinct frequency-dependent decrease in impedance with biofilm formation (N = 3). The large error bars arise due to the inherent variability of biofilm, and the presence of small bubbles.

compared to the bacteria free control (Fig. 5(c)) at 10 Hz (p = 0.1901), 100 Hz (p = 0.0947), 1 kHz (p = 0.0553), 10 kHz (p = 0.0020), and 100 kHz (p = 0.0715). This result suggests that the frequency-dependent decrease arises as the biofilm alters the double-layer capacitance in the circuit. The growth of a biofilm accumulates charged metabolites and ions at the electrode surface, leading to the decrease of the Debye length. This drives the increase in the double-layer capacitance corresponding to the frequency-dependent impedance decrease. These results are supported by similar electrical characteristics of biofilm seen in previous works [18], [42]. This conclusion could be further evaluated by comparing the impedance spectrum to various equivalent circuit models of biofilm growth, and examining the impedance shift with certain elements removed, such as mutant bacteria which do not attach and produce biofilm.

Furthermore, the real-time sensing capabilities of this flexible system were demonstrated, representing a significant advantage over present biofilm analysis techniques. To do so, the impedance at 100 Hz was tracked over the 24 hour growth period continuously to evaluate the real-time degree of biofilm formation. 100 Hz was selected as it showed highest sensitivity within the frequency range investigated, as shown in Fig. 5(d). The 100 Hz samples showed the largest change between the biofilm and unseeded control in the impedance spectra. The percent change relative to the initial system impedance was calculated and compared for devices with biofilm formation to unseeded controls. When bacteria were introduced into the device, biofilm formed on the surface and drove a decrease in the system impedance. The time-lapse images in Fig. 6(a), along with their corresponding impedance sensor signals in Fig. 6(b),
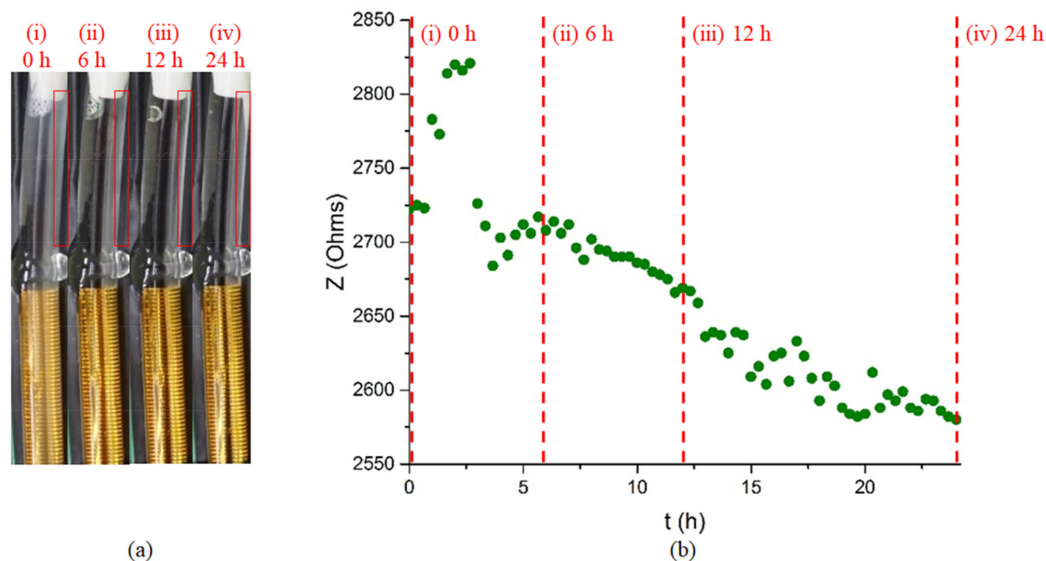
Fig. 6. (a) Time lapse images of platform in catheter tube, with the device in orange and the biofilm forming as a white streak along the edge of the tube in the red boxed region. (b) Impedance transient with lines indicating the impedance at each image. The initial spike in impedance is attributed to a small air pocket being flushed out of the tubing and passing over part of the sensor.

indicate a correlation between this drop in impedance and the rapid expansion of the biofilm colony. The biofilm can be seen in the red boxes in Fig. 6(a) growing in a layer on the side of the catheter tube. The start of the growth phase at t = 0 ((i) in Fig. 6) shows no biofilm and an impedance of 2.72 kΩ. An initial layer appears after 6 hours ((ii) in Fig. 6), showing only a slight decrease in impedance relative to the impedance at t = 0. After 12 hours ((iii) in Fig. 6) a thin layer of biofilm is visible, accompanied by a distinct drop in the impedance. The impedance decreases to 2.58 kΩ after 24 hours ((iv) in Fig. 6) with a thick, mature biofilm present.

The unseeded control, which has no bacteria to form a biofilm, showed a slight increase in impedance over the duration of the experiments (Fig. 7). As described previously, this is attributed to the formation of small air bubbles on the sensor surface. Conversely, when bacteria are introduced into the tube, a biofilm forms, leading to a dramatic 30% decrease in the impedance (Fig. 7) after 24 hours of growth. Similar to the above images, biofilm does not grow uniformly. On average, the impedance drops precipitously as the biofilm matures from initial colonization to the rapid proliferation phase. The impedance decreases 7.2% per hour from hour 2 to 3. However, there is a reduction in the rate of impedance decrease after this initial drop, as mature biofilms form and growth decelerates; from hour 3 to 24 the impedance decreases approximately 1% per hour. This result suggests a rapid proliferation phase followed by a slower-growing mature biofilm phase.

Impedance changes measured with the AD5933 impedance converter are depicted in Fig. 8. The trends produced reflect the similar sensing characteristics measured with the potentiostat for both control and biofilm samples. The biofilm-free samples yielded a slight increase in impedance after the 24-hour growth period of approximately 2%. By comparison, biofilm formation
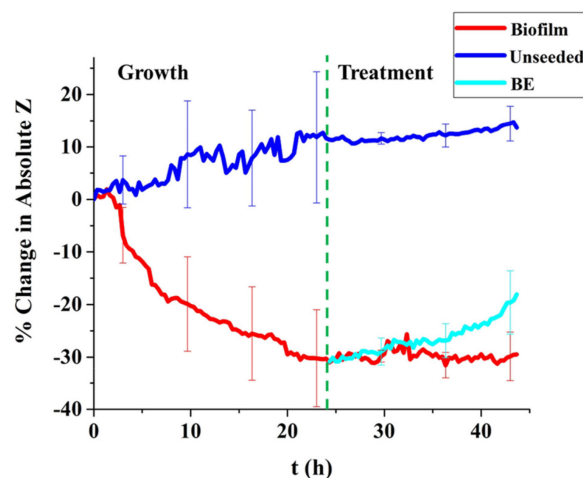

Fig. 7. Growth (left): Percent change in 50-mV impedance at 100 Hz for biofilm (red) and unseeded (blue) samples over a 24 hours growth period showing an initial drop followed by slowed growth. The large standard error indicates the high inherent variability of biofilm formation (N = 5). Treatment (right): Percent change in 50 mV 100 Hz impedance over the course of a 20-hour treatment period on a mature biofilm (i.e., relative to the impedance at the end of the growth phase). Removal of biofilm via BE led to a 12% increase in impedance compared with the 1% decrease for the sensing-only samples (N = 3).

led to a drop of about 5% in the measured impedance after 24 hours of growth. The most notable difference between the results with the AD5933 and the standard benchtop potentiostat is the decreased magnitude of the changes in impedance for both samples. The signal change equated to only 16% of the average percent change seen over the same period using the potentiostat. This decreased sensitivity is likely attributed to differences in system calibration and variations in impedance of the measurement electronics. Nonetheless, the similar trend
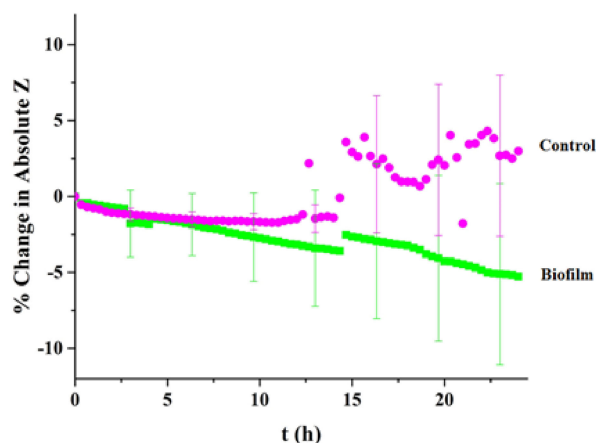
Fig. 8. Percent change in 200-mV impedance at 1 kHz measured with the AD5933 impedance converter for biofilm (green) and control (pink) samples over a 24-hour growth period showing a steady drop associated with biofilm growth. The large standard error indicates the high inherent variability of biofilm formation (N = 3).
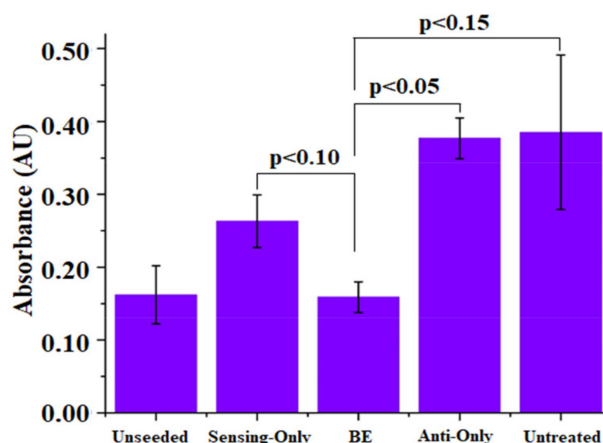

Fig. 9. CV staining to evaluate the biomass at the end of each of the five treatments showing the decrease in biofilm due to BE: Unseeded, Sensing-Only, Anti-Only, and Untreated, and BE. (N = 3).

versus the standard indicates that biofilm detection with AD5933 is feasible.

In order to fully implement this approach, several steps must be taken including: 1) integration of electrodes with a functional urinary catheter, 2) development of software to perform automated measurement and response, 3) optimization of electronics, and 4) miniaturization of an external electronics module including power and wireless components. Some technical challenges associated with this include 1) calibration of wireless sensor response, 2) interfacing the internal electrodes with the external electronics, and 3) minimizing the impact of the physical footprint of the electronics module on regular system performance.

B. Bioelectric Effect Treatment

A secondary component of this platform is the capability to implement BE treatment using the same electrodes and electrical signals that are used for impedance sensing (Fig. 7). Following the formation of a mature biofilm during the 24-hour growth period, the flexible electrode system was used to apply a BE-based treatment. This utilized gentamicin diluted in the LB growth media to the concentration of 10 μg/ml, combined with the same 50 mV AC signal utilized for sensing to achieve synergistic biofilm removal. This 50 mV signal maintained a similar electric field strength compared to our previous work where the BE was implemented successfully in a microfluidic device [16]. The 50 mV signal alone (Sensing-Only) showed a 1% decrease in impedance during the treatment period relative to the impedance at the end of the 24-hour growth phase, indicative of negligible change in biofilm. However, when the synergistic BE treatment was applied, the sensor measured a 12% increase in impedance relative to the initial impedance of the mature biofilm at the start of the treatment phase/end of the growth phase. This suggests effective removal of the biofilm via BE which has led to an increase in impedance because the film was no longer able to adhere strongly to the surface or accumulate ions after treatment.

C. Biomass Quantification

A CV absorbance assay was performed to quantify the amount of strongly adhered biofilm material on the surface of the tube following the treatment period (Fig. 9). The untreated control, without the sensing signal or antibiotics, presented an average absorbance of 0.385 ± 0.106. This decreased to 0.159 ± 0.021 for the BE treatment group, similar to the 0.143 ± 0.023 absorbance found with the unseeded control. The absorbance for the untreated control is attributed to the conditioning layer from the LB media. The antibiotic-only group showed an absorbance of 0.377 ± 0.028, while the sensing-only group had an absorbance of 0.263 ± 0.036. The small decrease for the sensing-only group suggests that the electric field may contribute in reducing biofilm slightly. BE treatment yielded a significant decrease in biomass compared to the antibiotic-only sample (ANOVA $p < 0.05$). This data also indicates a distinct trend showing the decrease in biomass from untreated or sensing-only samples to BE treatment (ANOVA $p = 0.1054$ and $p = 0.0663$, respectively). The unseeded control absorbance corresponded to the signal attributed to the presence of pure LB media, and the similar absorbance after 24 hours of BE treatment indicated there was a negligible amount of adhered biomass remaining in the tube. The unseeded samples displayed significantly less biomass when compared with the sensing-only ($p = 0.04693$), antibiotic-only ($p = 0.00287$), or untreated ($p = 0.08976$) groups. There appeared to be less biomass than the controls with the electric field or antibiotic alone, highlighting the synergistic effect of the treatment. Previous work suggests that the electrical energy of the sensing signal allows either an increase in the permeability of the bacterial cell membrane, enhanced diffusion of the charged antibiotic, or both [43]. This serves to explain the increased efficacy of antibiotics in reducing biofilm in the presence of the electric field introduced by this flexible platform.

IV. Conclusion

Two disparate functions were demonstrated with this flexible platform: 1) real-time biofilm formation monitoring via

impedance sensing, and 2) biofilm treatment utilizing BE. These are achieved through simple gold IDEs fabricated on a flexible polyimide substrate. Biofilm growth was characterized by a dramatic, frequency-dependent drop in system impedance, which was used to monitor a catheter surface in real-time. The 30% decrease at 100 Hz over 24 hours of growth was correlated with biomass and optical images, confirming the utility of this platform as an effective and reliable monitoring tool. In addition, sensing was performed using the AD5933 impedance converter allowing miniaturization. Biofilm formation resulted in a 5% impedance decrease when measured with the AD5933. This change corresponded with the trend seen with the potentiostat, but had a six-fold smaller magnitude. Along with wireless control, this is an invaluable element for implementation of this platform in situ for complex and inaccessible surfaces. Furthermore, the sensing electric field generated by the IDEs was shown to be capable of inducing the BE when combined with a low dosage of gentamicin treatment. BE treatment led to an increase in impedance of 12%, along with a decrease in biomass to levels similar to unseeded samples. Thus, this approach demonstrated effective biofilm infection management without relying on excessive antibiotic dosages.

The conformable nature of the device enables integration with complex, 3D vulnerable surfaces for in situ biofilm management. While this work demonstrates this in the cylindrical domain of a urinary catheter, this can be extended to geometries associated with other domains that are particularly vulnerable, such as prosthetic implants, water system components, or dental devices. Furthermore, testing with other bacterial species, including clinical isolates, in a range of fluidic environments like pooled urine will serve to expand this approach toward in vivo implementation and clinical trials.

ACKNOWLEDGMENT

REFERENCES

[1] H.-C. Flemming *et al.*, "Biofilms: An emergent form of bacterial life," *Nature Rev. Microbiol.*, vol. 14, no. 9, pp. 563–575, 2016.

[2] J. W. Costerton *et al.*, "Bacterial biofilms: A common cause of persistent infections," *Science*, vol. 284, no. 5418, pp. 1318–1322, 1999.

[3] H. Anwar *et al.*, "Testing the susceptibility of bacteria in biofilms to antibacterial agents," *Antimicrobial Agents Chemotherapy*, vol. 34, no. 11, pp. 2043–2046, 1990.

[4] M. Habash and G. Reid, "Microbial biofilms: Their development and significance for medical device-related infections," *J. Clin. Pharmacol.*, vol. 39, no. 9, pp. 887–898, 1999.

[5] S. S. Magill *et al.*, "Multistate point-prevalence survey of health care–associated infections," *New England J. Med.*, vol. 370, no. 13, pp. 1198–1208, 2014.

[6] J. W. Warren, "Catheter-associated urinary tract infections," *Int. J. Antimicrobial Agents*, vol. 17, no. 4, pp. 299–303, 2001.

[7] A. Vendeville *et al.*, "Making 'sense' of metabolism: Autoinducer-2, LUXS and pathogenic bacteria," *Nature Rev. Microbiol.*, vol. 3, no. 5, pp. 383–396, 2005.

[8] R. O. Darouiche, "Treatment of infections associated with surgical implants," *New England J. Med.*, vol. 350, pp. 1422–1429, 2004.

[9] D. G. Maki *et al.*, "A semiquantitative culture method for identifying intravenous-catheter-related infection," *New England J. Med.*, vol. 296, no. 23, pp. 1305–1309, 1977.

[10] E. Peeters *et al.*, "Comparison of multiple methods for quantification of microbial biofilms grown in microtiter plates," *J. Microbiol. Methods*, vol. 72, no. 2, pp. 157–165, 2008.

[11] R. J. Palmer and C. Sternberg, "Modern microscopy in biofilm research: Confocal microscopy and other approaches," *Current Opinion Biotechnol.*, vol. 10, no. 3, pp. 263–268, 1999.

[12] Y. W. Kim *et al.*, "An ALD aluminum oxide passivated Surface Acoustic Wave sensor for early biofilm detection," *Sensors Actuators, B. Chem.*, vol. 163, no. 1, pp. 136–145, 2012.

[13] K. Waszczuk *et al.*, "Evaluation of Pseudomonas aeruginosa biofilm formation using piezoelectric tuning fork mass sensors," *Sensors Actuators, B. Chem.*, vol. 170, pp. 7–12, 2012.

[14] M. T. Meyer *et al.*, "Development and validation of a microfluidic reactor for biofilm monitoring via optical methods," *J. Micromech. Microeng.*, vol. 21, no. 5, 2011, Art. no. 54023.

[15] Y. W. Kim *et al.*, "MIcrofluidic biofilm observation, analysis and treatment (MICRO-BOAT) platform," in *Proc. Tech. Digest—Solid-State Sensors, Actuators, Microsyst. Workshop*, 2012, pp. 233–236.

[16] S. Subramanian *et al.*, "An integrated microsystem for real-time detection and threshold-activated treatment of bacterial biofilms," *ACS Appl. Mater. Interfaces*, vol. 9, pp. 31362–31371, 2017.

[17] J. Paredes *et al.*, "Interdigitated microelectrode biosensor for bacterial biofilm growth monitoring by impedance spectroscopy technique in 96-well microtiter plates," *Sensors Actuators, B Chem.*, vol. 178, pp. 663–670, 2013.

[18] J. Paredes *et al.*, "Real time monitoring of the impedance characteristics of Staphylococcal bacterial biofilm cultures with a modified CDC reactor system," *Biosensors Bioelectron.*, vol. 38, no. 1, pp. 226–232, 2012.

[19] X. Muñoz-Berbel *et al.*, "On-chip impedance measurements to monitor biofilm formation in the drinking water distribution network," *Sensors Actuators, B Chem.*, vol. 118, no. 1/2, pp. 129–134, 2006.

[20] J. Paredes *et al.*, "Label-free interdigitated microelectrode based biosensors for bacterial biofilm growth monitoring using Petri dishes," *J. Microbiol. Methods*, vol. 100, no. 1, pp. 77–83, 2014.

[21] L. Yang and R. Bashir, "Electrical/electrochemical impedance for rapid detection of foodborne pathogenic bacteria," *Biotechnol. Adv.*, vol. 26, pp. 135–150, 2008.

[22] K. K. Chung *et al.*, "Impact of engineered surface microtopography on biofilm formation of Staphylococcus aureus," *Biointerphases*, vol. 2, no. 2, pp. 89–94, 2007.

[23] N. Maccallum *et al.*, "Liquid-infused silicone as a biofouling-free medical material," *ACS Biomater. Sci. Eng.*, vol. 1, no. 1, pp. 43–51, 2015.

[24] H. Qin *et al.*, "In vitro and in vivo anti-biofilm effects of silver nanoparticles immobilized on titanium," *Biomaterials*, vol. 35, no. 33, pp. 9114–9125, 2014.

[25] M. N. Mann *et al.*, "Plasma-modified nitric oxide-releasing polymer films exhibit time-delayed 8-log reduction in growth of bacteria," *Biointerphases*, vol. 11, no. 3, 2016, Art. no. 31005.

[26] A. Yu Nikiforov *et al.*, "Atmospheric pressure plasma deposition of antimicrobial coatings on non-woven textiles," *Eur. Phys. J. Appl. Phys.*, vol. 75, pp. 1–6, 2016.

[27] J. Chen *et al.*, "An immobilized liquid interface prevents device associated bacterial infection in vivo," *Biomaterials*, vol. 113, pp. 80–92, 2017.

[28] V. Roy *et al.*, "AI-2 analogs and antibiotics: A synergistic approach to reduce bacterial biofilms," *Appl. Microbiol. Biotechnol.*, vol. 97, no. 6, pp. 2627–2638, 2013.

[29] V. Roy *et al.*, "Synthetic analogs tailor native Al-2 signaling across bacterial species," *J. Amer. Chem. Soc.*, vol. 132, no. 32, pp. 11141–11150, 2010.

[30] S. Subramanian *et al.*, "Autoinducer-2 analogs and electric fields—An antibiotic-free bacterial biofilm combination treatment," *Biomed. Microdevices*, vol. 18, no. 5, pp. 1–12, 2016.

[31] S. T. Sultana *et al.*, "Electrochemical scaffold generates localized, low concentration of hydrogen peroxide that inhibits bacterial pathogens and biofilms," *Sci. Rep.*, vol. 5, 2015, Art. no. 14908.

[32] J. W. Costerton *et al.*, "Mechanism of electrical enhancement of efficacy of antibiotics in killing biofilm bacteria," *Antimicrobial Agents Chemotherapy*, vol. 38, no. 12, pp. 2803–2809, 1994.

[33] B. Jaideep *et al.*, "Silver-Zinc redox-coupled electroceutical wound dressing disrupts bacterial biofilm," *PLoS One*, vol. 10, no. 3, pp. 1–15, 2015.

[34] K. G. Barki *et al.*, "Electric field based dressing disrupts mixed-species bacterial biofilm infection and restores functional wound healing," *Ann. Surg.*, vol. 269, no. 4, pp. 756–766, Apr. 2019.

[35] S. T. Sultana *et al.*, "Electrochemical biofilm control: A review," *Biofouling*, vol. 31, no. 9, pp. 745–758, 2015.

[36] S. A. Blenkinsopp *et al.*, "Electrical enhancement of biocide efficacy against Pseudomonas aeruginosa biofilms," *Appl. Environ. Microbiol.*, vol. 58, no. 11, pp. 3770–3773, 1992.

[37] P. S. Stewart *et al.*, "Electrolytic generation of oxygen partially explains electrical enhancement of tobramycin efficacy against Pseudomonas aeruginosa biofilm," *Antimicrobial Agents Chemotherapy*, vol. 43, no. 2, pp. 292–296, 1999.

[38] B. R. Mcleod *et al.*, "Enhanced bacterial biofilm control using electromagnetic fields in combination with antibiotics," *Methods Enzymol.*, vol. 310, pp. 656–670, 1999.

[39] M. E. Shirtliff *et al.*, "Assessment of the ability of the bioelectric effect to eliminate mixed-species biofilms," *Appl. Environ. Microbiol.*, vol. 71, no. 10, pp. 6379–6382, 2005.

[40] Y. W. Kim *et al.*, "A surface acoustic wave biofilm sensor integrated with a treatment method based on the bioelectric effect," *Sensors Actuators A Phys.*, vol. 238, pp. 140–149, 2016.

[41] J. M. Seo *et al.*, "Biocompatibility of polyimide microelectrode array for retinal stimulation," *Mater. Sci. Eng. C*, vol. 24, no. 1/2, pp. 185–189, 2004.

[42] K. G. Ong *et al.*, "Monitoring of bacteria growth using a wireless, remote query resonant-circuit sensor: Application to environmental sensing," *Biosensors Bioelectron.*, vol. 16, no. 4/5, pp. 305–312, 2001.

[43] Y. W. Kim *et al.*, "Effect of electrical energy on the efficacy of biofilm treatment using the bioelectric effect," *NPJ Biofilms Microbiomes*, vol. 1, 2015, Art. no. 15016.